Modeling of Shape Memory Alloy pseudoelastic spring elements using Preisach model for passive vibration isolation

Mughees M. Khan[a] and Dimitris C. Lagoudas[a]

[a]Active Materials Laboratory
Department of Aerospace Engineering, Texas A&M University, College Station, TX-77843

ABSTRACT

Advances in active materials and smart structures, especially in applications of Shape Memory Alloys (SMA) as vibration isolation devices requires modeling of the pseudoelastic hysteresis found in SMAs. In general SMA hysteresis has been modeled either through constitutive models based on mechanics and material parameters or through system identification based models that depend only on input-output relationships, most popular being the Preisach Model. In this work, a basis is set forth for studying the effect of SMA pseudoelasticity on the behavior of vibrating systems. A Preisach Model is implemented to predict the component level pseudoelastic response of SMA spring elements. The model is integrated into a numerical solution of the non-linear dynamic system that results from the inclusion of Shape Memory Alloy components in a dynamic structural system. The effect of pseudoelasticity on a dynamic system is investigated for various loading levels and system configurations and the importance of large amplitude motion is discussed. Promising results are obtained from these investigations and the application of these studies to experimental work in progress by the authors is briefly discussed.

Keywords: Shape Memory Alloys (SMA), Pseudoelasticity, Hysteresis, Preisach, System Identification, Vibration Isolation, Dynamic System

1. INTRODUCTION

The goal of vibration isolation is to reduce the force or motion transmitted from one structure to another, which is most commonly accomplished through the use of an isolation system with a relatively small stiffness[1] . However, for isolation of heavy loads, a small stiffness will lead to large displacements. This large displacement obstacle has often been overcome through the use of a device with decreasing stiffness, like a softening spring. Such a device would have a very stiff initial response that becomes less stiff as the load is increased, so that the stiff region of the device's response supports the initial load and the transmissibility is reduced by the lower stiffness in the operating range. One of the problems encountered in vibration isolation using a softening spring is resonant behavior at low excitation frequencies, where the soft nature of the stiffness shifts the natural frequency to lower frequencies. This condition has lead to addition of some type of damping to the system, which has the desired effect of decreasing the resonant response but also degrades the response of the isolator at higher frequencies as shown by Harris[2] . Therefore, the task of damping and vibration isolation is often faced with trade-offs. The use of shape memory alloys(SMAs) may allow for the elimination of these trade-offs, resulting in better performance with fewer compromises as the behavior of devices with decreasing stiffness and a damper is similar to the hysteretic load-deflection relationship exhibited by SMAs during pseudoelastic deformation[3] as discussed later.

The pseudoelastic behavior of SMAs is defined as, inducing martensitic phase transformation by a mechanical loading (stress induced martensite), while the material is in austenitic phase. The mechanical loading, forces martensitic variants to reorient (detwin) into a single variant, resulting in relatively large macroscopic strains, and these strains can be fully recovered upon unloading to the zero-stress state[4–6] . Figure 1 presents a typical

Further author information: (Send correspondence to D.C.L.)
D.C.L.: E-mail: dlagoudas@aero.tamu.edu, Telephone: 1 (979) 845-1604
M.M.K.: E-mail: mkhan@tamu.edu, Telephone: 1 (979) 845-0716

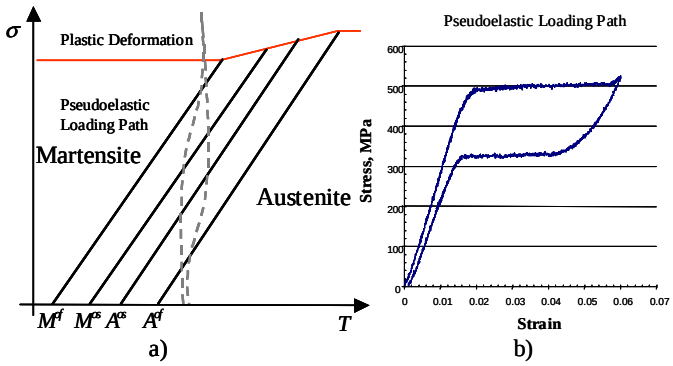

Figure 1. a) Typical SMA phase diagram with a typical pseudoelastic loading path noted in stress-temperature space b) Corresponding pseudoelastic loading path in stress-strain space

SMA phase diagram, showing the relationship between stress, temperature, and phase and a typical pseudoelastic loading path discussed above. The transformation temperatures at the zero-stress state are represented as M^{0s},M^{0f},A^{0s} and A^{0f} in Figure 1. In addition to the change in material properties and large recoverable strain during pseudoelastic transformation, there is some hysteresis which is an indicator of energy dissipation during the austenite to martensite and martensite to austenite transformations. This energy dissipation is proportional to the degree of transformation completed during a loading cycle for both complete and incomplete, or partial, transformations. These partial transformations are also referred to as minor loop hysteresis cycles[7] and complete, or full transformations are referred to as major loop hysteresis cycles. The energy dissipation due to hysteresis provide an opportunity for SMAs to be used as damping devices and the change in the tangent stiffness of the material during pseudoelastic phase transformations provide opportunities for SMAs to be used as vibration isolation devices.

The nature of the pseudoelastic effect, as discussed above and illustrated in Figure 1b, indicates great potential in the application of SMAs to vibration isolation, especially since SMAs can also be used to provide structural support rather than just used as damping and vibration isolation devices. This has added benefits in terms of having relatively simple, lightweight and compact devices. Utilization of SMAs for such applications requires understanding of the nonlinear hysteretic response found in SMAs. Graesser and Cozzarelli[8] introduced a model for hysteretic behavior, a modification of the model introduced by Ozdemir[9] to model pseudoelastic behavior of SMAs, using ideas from viscoplasticity based on work done by Achenbach[10] and applied the results to seismic isolation of structures. A study on the use of SMAs for passive structural damping is presented in Thompson et al.,[11] where three different quasi-static models of hysteresis were introduced and compared with an experimental investigation of a cantilevered beam constrained by two SMA wires. In work done by Feng and Li,[12] another example of passive vibration damping using SMAs is presented, where a modified plasticity model[8] is used to model the pseudoelastic response of an SMA bar in place of a spring in a single degree of freedom (SDOF) spring mass damper system. Fosdick and Ketema,[13] have considered rate dependency by including "averaged" thermal effects, their work is based on dynamics of single-crystal phase boundaries by Abeyaratne et al.,[14] and they have studied a SDOF lumped mass oscillator with an SMA wire attached in parallel as a passive vibration damper.

However, studies of the models available in literature and their utilization for various SMA based smart structure applications reveal that although these models are quite accurate, they are computationally intensive and/or hard to implement under dynamic loading conditions. Additionally, the nature of the pseudoelastic effect as it can be applied to vibration isolation and damping through the utilization of SMAs has not been addressed by the above publications. A noted exception is the work of Yiu and Regelbrugge[15] , whose work investigated the behavior of SMA springs designed to act as an on-orbit soft mount isolation system for a momentum wheel assembly with the added benefit of precision alignment through the utilization of the shape memory effect.

Motivated by the need to model a prototype of an SMA based isolation system[16] , a dynamic system with SMA spring components is investigated through numerical simulation in this work. To realize the goal of

designing and simulating a smart structure for vibration isolation using SMAs, it is necessary to have structural models that can (a) incorporate response of SMAs and (b) can be used for prediction of dynamic response of smart structures. Most of the models available in the literature do not serve this dual purpose well. In earlier work presented by the authors[17] , the effect of the hysteresis and softening stiffness exhibited during pseudoelasticity on a dynamic system is predicted through the use of a numerical simulation of the dynamic system which consists of a structural model of the dynamic system coupled with a computationally efficient physically based material model for SMA pseudoelasticity. The model presented in Ref. 17 has been utilized to perform parametric studies for an SMA based passive vibration isolation device. However, for performing design optimization and simulation of a specific dynamic system[16] the generality and computational efficiency of a system identification (ID) based model is necessary.

In this work a Preisach model, an empirical model based on system ID is developed for pseudoelastic SMA spring elements in order to have accurate and efficient modeling for performing design optimization and simulation of the dynamic system presented in Ref. 16. A computationally efficient scheme that also minimizes noise due to identification experiments has been implemented. The model is coupled with an implicit integration scheme to solve a SDOF passive vibration isolation system having SMA spring elements. The following section (Sec. 2) will discuss the adaptation of the classical Preisach model to the pseudoelastic behavior of SMA spring elements, the experiments performed to identify the Preisach model and comparison of the calibrated model with the actual SMA spring element response. Sec. 3 will discuss the application of the model to a SDOF SMA spring(s) mass system followed by simulation results and conclusions.

2. DEVELOPMENT OF PREISACH MODEL FOR PSEUDOELASTIC SMA SPRING ELEMENT

2.1. Adaptation of Classical Preisach Model for Pseudoelastic SMA Spring Elements

The classical Preisach model can be expressed as a weighted combination of relay operators[18] . Figure 2a shows a classical Preisach hysteresis relay operator $H_{\alpha\beta}[\delta(t)]$. The relay operator can be explained by a rectangular loop where α and β correspond to "up" and "down" switching values of the input respectively and it is assumed that $\alpha \geq \beta$. The rectangular loop can also be associated as a simplified representation of actual pseudoelastic SMA response. Work done by Webb[19, 20] have shown that a Krasnoselskii-Pokrovskii (KP)[21] type of hysteresis operator, gives a better representation of SMA response. The KP type operator is an hysteretic operator with continuous branches rather than jump discontinuities like the Preisach operator. As a first step, a modified Preisach operator is implemented in this work, to account for pseudoelastic SMA spring element response rather than the KP operator for simplicity in implementation.

To summarize, the Preisach model consists of hysteretic operators, where each operator's output is either $+1$ or -1 based on the value of the input. The operator output and input values are governed by the position of the system or material response in the planar quadrants. As shown in Figure 1, the SMA pseudoelastic response can be represented either in the first or the third quadrant depending on the SMA element response. In this work, the SMA element response corresponds to SMA spring element undergoing tension or compression. Therefore, due to the type of hysteresis found in SMA pseudoelasticity, the output value of the hysteresis operator used in this work have been modified to 0 or 1, as shown in Figure 2b.

The mathematical form of the classical Preisach model is given as

$$f^{SMA}(t) = \iint_{\alpha \geq \beta} \mu(\alpha, \beta) H_{\alpha\beta}[\delta(t)] d\alpha d\beta \tag{1}$$

where $\delta(t)$ is the input and represents displacement for the SMA spring elements, $H_{\alpha\beta}[\delta(t)]$ represents hysteresis relay operators with different α and β values containing the hysteresis effects and depends on $\delta(t)$. Here α and β correspond to increasing and decreasing values of displacement. $\mu(\alpha, \beta)$ represents weighing function in the Preisach model, it describes the relative contribution of each relay to the overall hysteresis and $f^{SMA}(t)$ is the output representing force generated by the SMA spring element and depends on the displacement history. The

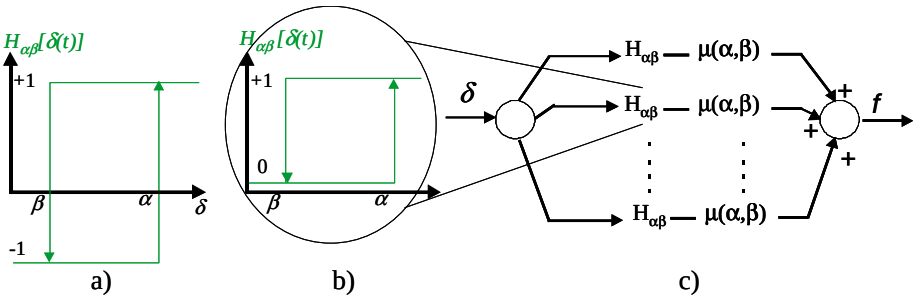

Figure 2: a) Classical hysteresis operator b) Modified hysteresis operator c) Schematic of Preisach model

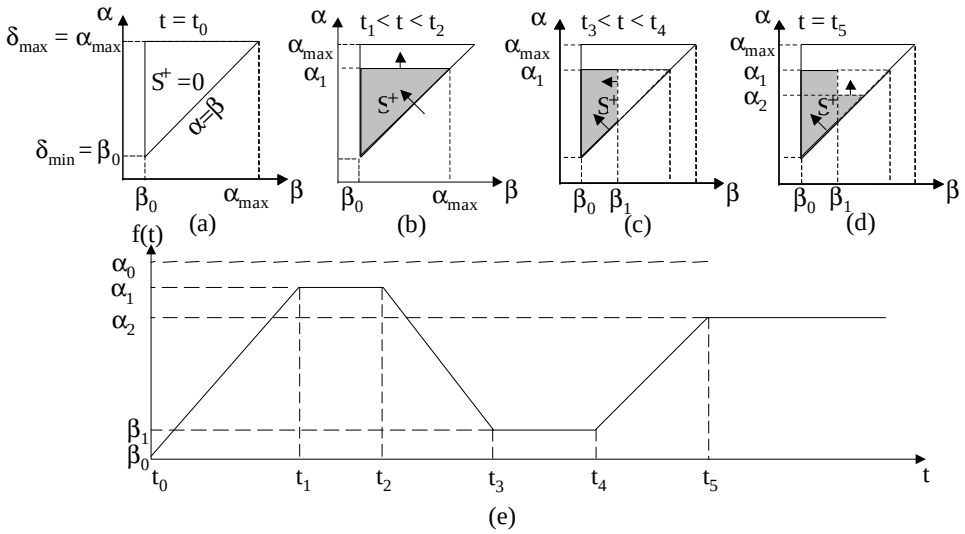

Figure 3: Evolution of outputs over the Preisach plane

double integration presented in Equation 1 can be interpreted as a parallel summation of weighted relays as shown in Figure 2c.

The weighting function $\mu(\alpha, \beta)$, also referred in the literature as the preisach function is described over a region P, this region is referred to as the Preisach plane, where each point in P represents a unique relay. Based on the explanation given on the Preisach Model in Ref. 18, 22, 23, the weighting function is defined over displacement(input) range, i.e the domain of hysteresis exists between δ_{min} and δ_{max}. α and β represents increasing and decreasing displacement values respectively, where the upper bound on α is given by δ_{max} and the lower bound on β is given by δ_{min}. These two conditions along with the condition given in Equation 1, which defines the double integration to exist over a surface where $\alpha \geq \beta$, restricts P to a triangle. Figure 3a shows the schematic of the preisach plane adapted for the work presented in this paper.

It must be noted that, according to Figure 2, $H_{\alpha,\beta}[\delta(t)]$ can only take the values 0 and 1. Thus, the Equation 1 (1) reduces to,

$$f^{SMA}(t) = \iint_{S^+(t)} \mu(\alpha, \beta) d\alpha d\beta \tag{2}$$

where S^+ is the region (in the shaded support $\alpha \geq \beta$ shown in Figure 3) containing all the relays operators in +1 state at time t. The other relays outside the shaded area are in zero state. There is a one-to-one correspondence between the relays $H_{\alpha,\beta}$ and the points (α, β) within triangle area $(\alpha \geq \beta)$.

Figure 3 shows the geometrical interpretation of the Preisach model, it can be seen that the integration

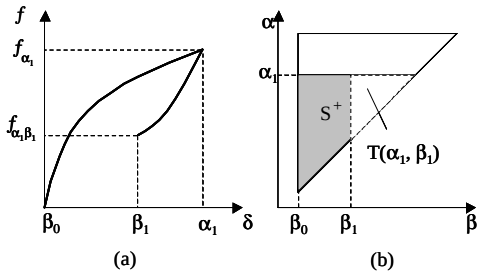

Figure 4: Schematic of identification input

support area is changing with the change in input direction. Not all the input directional changes or input reversal points are remembered by the model. The input maximum wipes out the vertices whose α co-ordinates are below this input, and each input minimum wipes out the vertices whose β are above this minimum. This in essence shows dependency of output on previous dominant input extrema and represents the loading path dependency as demonstrated by the pseudoelastic SMA response.

2.1.1. Identification of the Preisach function

The Preisach function or the weighting surface for any hysteretic system in this case an SMA spring element can be easily determined from experimental data. This experimental data must contain what is defined as "first-order transition" (FOT) curves. The procedure is as follows. First, the input $\delta(t)$ is brought to its minimum δ_{min} which is represented as β_0 in Figure 4a. Then monotonically increased to some value α_1, as the input is increased from δ_{min}, an ascending branch of a major loop is followed, which is also referred to as a limiting branch in the literature.[18] f_{α_1} represents the output corresponding to α_1, the input is now decreased monotonically to a value β_1 and the corresponding output is described as $f_{\alpha_1\beta_1}$. The term first-order describes that such curves are obtained after the first reversal of input. Note that FOT can also be obtained by first-order descending curves as well. The corresponding $\alpha - \beta$ diagram is shown in Figure 4b. To derive the weighting function in terms of FOT curves we introduce a function $F(\alpha_1, \beta_1)$,

$$F(\alpha_1, \beta_1) = f_{\alpha_1} - f_{\alpha_1\beta_1} \tag{3}$$

which represents the change in force as the displacement changes from α_1 to β_1. Equation 3 can also be represented as

$$F(\alpha_1, \beta_1) = \iint\limits_{T(\alpha_1,\beta_1)} \mu(\alpha, \beta) d\alpha d\beta \tag{4}$$

The weighing function is obtained by taking the partial derivatives of Equation 4.

$$\mu(\alpha_1, \beta_1) = -\frac{F(\alpha_1, \beta_1)}{d\alpha_1 d\beta_1} \tag{5}$$

However, in order to avoid the double numerical differentiation of $F(\alpha_1, \beta_1)$ to obtain $\mu(\alpha_1, \beta_1)$, the function $F(\alpha_1, \beta_1)$ itself, is used to obtain the expression for the force, rather than Equation 2. This helps in avoiding amplifying errors in the experimental data and simplifies the numerical implementation of the Preisach model.

Explicit expressions for force in terms of $F(\alpha_1, \beta_1)$ can be subdivided into subcases based on increasing and decreasing displacement. For an increasing displacement(Figure 5a) , $f^{SMA}(t)$ is a double integral of the weighted function $\mu(\alpha, \beta)$ on a region circumscribed by a set of links whose final segment is a horizontal line as shown in Figure 5b. Starting from Equation 2 we can represent $f^{SMA}(t)$ as

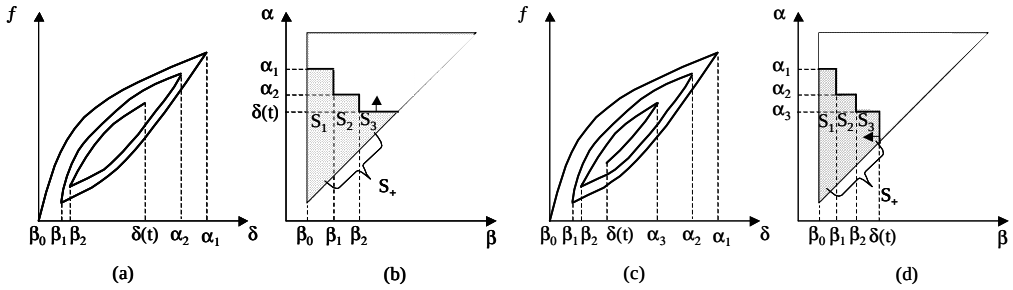

Figure 5: Schematic for increasing and decreasing inputs

$$
\begin{aligned}
f^{SMA}(t) &= \iint_{S_1(t)} \mu(\alpha,\beta)d\alpha + \iint_{S_2(t)} \mu(\alpha,\beta)d\alpha + \iint_{S_3(t)} \mu(\alpha,\beta)d\alpha d\beta \\
&= [F(\alpha_1,\beta_0) - F(\alpha_1,\beta_1)] + [F(\alpha_2,\beta_1) - F(\alpha_2,\beta_2)] + F(\delta(t),\beta_2) \\
&= \sum_{k=1}^{N} [F(\alpha_k,\beta_{k-1}) - F(\alpha_k,\beta_k)] + F(\delta(t),\beta_k) \qquad (6)
\end{aligned}
$$

where the integration is equivalent to summation of the trapezoids within the $S^+(t)$ region, which can be generalized as shown in Equation 6.

Similarly, for decreasing displacement as shown in Figure 5c, $f^{SMA}(t)$ is a double integral of the weighted function $\mu(\alpha,\beta)$ on a region circumscribed by a set of links whose final segment is a vertical line as shown in Figure 5d. Starting from Equation 2 we can represent $f^{SMA}(t)$ as

$$
\begin{aligned}
f^{SMA}(t) &= [F(\alpha_1,\beta_0) - F(\alpha_1,\beta_1)] + [F(\alpha_2,\beta_1) - F(\alpha_2,\beta_2)] \\
&\quad +[F(\alpha_3,\beta_2) - F(\alpha_3,(\delta(t)) \\
&= \sum_{k=1}^{N-1} [F(\alpha_k,\beta_{k-1}) - F(\alpha_k,\beta_k)] + [F(\alpha_N,\beta_{N-1}) - F(\alpha_N,(\delta(t))] \qquad (7)
\end{aligned}
$$

Equations 6 and 7 give the necessary increasing and decreasing displacement expression in terms of the measured FOT data. The following subsection discusses the FOT data collection and the identified model.

2.2. FOT Data Collection and Model Identification

In order to perform the FOT data collection a pseudoelastic SMA spring element was loaded in compression. The spring element was subjected to a range of displacements [0,4]mm which corresponds to [δ_{min},δ_{max}] and represent the lower and upper bound on displacements. The displacement range was subdivided into 13 sub-ranges of orders pairs $\{\delta_i\}_{i=0,\ldots,n}$ leading to $\frac{n}{2}(n+3)$ FOT data points for all pairs (δ_i,δ_j) with $j \leq i$. Force-displacement tests were performed on an MTS servo-hydraulic load frame with a TestStar IIm controller under displacement control at 25^oC. The displacement input used for the FOT curves is given in Figure 6a and the corresponding force-displacemnt diagram is shown in Figure 6b. Figure 7a shows a 3-D plot of the FOT data obtained from Figure 6b.

Theoretically greater amount of FOT curves collected lead to more accurate hysteresis modeling, however this amounts to greater memory storage requirements and lower computational efficiency. Hence a trade-off needs to be exercised on accuracy compared to computational efficiency and since the objective is to have a computationally efficient model for predicting dynamic response, therefore only 90 FOT data points have been considered, this was the reason for having the displacement range subdivided into 13 sub-ranges. Figure 7b shows the experimental data along with the 90 data points used to generate $F(\alpha,\beta)$ function. The Preisach model simulated using the $F(\alpha,\beta)$ function is also shown in Figure 7b.

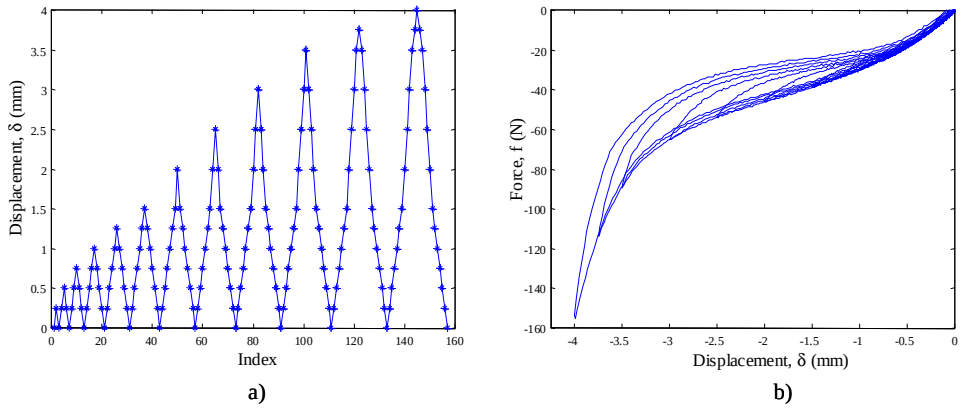

Figure 6: a) Identification displacement(input) b) Experimental FOT curves

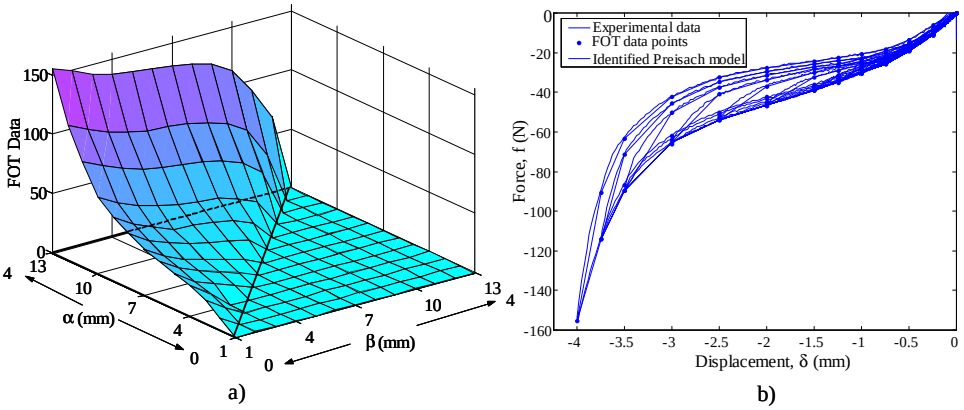

Figure 7: a) Experimental FOT data b) Identified Preisach model using 90 data points

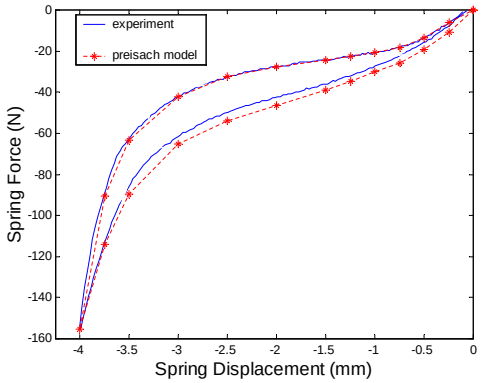

Figure 8: Comparison of calibrated model with experimental response

Figure 8 shows a comparison of the calibrated Preisach model response and the experimental SMA spring element response. To account for input displacements which do not correspond to any stored FOT curves, linear numerical interpolation has been used to determine the output force. The numerical implementation of the Preisach model was performed in MATLAB[24] . The following section discusses the application of the Preisach model to solve a SDOF SMA spring mass system.

3. APPLICATION OF PREISACH MODEL TO A PASSIVE VIBRATION ISOLATION SYSTEM

3.1. System Description

Motivated by the need to model a prototype of an SMA based isolation device[16] , the Preisach model is used to solve a coupled structural response involving SMAs. To determine the effect of pseudoelastic SMA springs on the response of a single degree of freedom (SDOF) spring-mass system, the system is modeled with the traditional linear springs replaced by non-linear, hysteretic SMA springs. These SMA springs operate in compression and are subjected to some degree of pre-compression prior to excitation so that the springs are operating in the middle of their pseudoelastic response. A schematic of the SMA spring-mass system along with a free-body diagram of the mass being isolated is shown in Figure 9. The system is excited by the motion of the supporting structure, denoted by (y)(Base displacement). From the free body diagram in Figure 9b, the equation of motion for the system can be determined as shown in Equation 8. (m) is the mass to be isolated, $(\ddot{x})$ is the acceleration of the isolated mass and (N_u) and (N_l) refer to the number of springs on the upper or lower sides of the mass, respectively. As SMA hysteresis is rate independent, therefore the forces exerted by the SMA springs not only account for the change in stiffness but also the damping introduced in the system. Therefore, there is no specific damping term in Equation 8. The forces exerted by the SMA springs, (f_u^{SMA}) and (f_l^{SMA}), the Force exerted by the upper springs and lower springs are determined by the displacement of the springs, (δ_u) and (δ_l), and the displacement history of the springs as discussed previously. These displacements are functions of (x)(Displacement of mass) and (y) as shown in Equation 9. It should be noted that due to the non-linear nature of the force-displacement relationship for these springs, both the upper springs and lower springs must be modeled independently of each other.

$$m\ddot{x} = N_u f_u^{SMA}[\delta_u] - N_l f_l^{SMA}[\delta_l] \tag{8}$$

$$\delta_l = -\delta_u = x - y \tag{9}$$

Excitation of the system is introduced through sinusoidal motion of the base of the device whose magnitude is determined by the desired loading to be placed on the structure. Loading magnitude,(a)(Input loading level) is specified as a fraction of the acceleration due to gravity, (g). Loading frequency is specified in cycles per second, denoted as (f) (Excitation frequency). The acceleration due to gravity is taken as $9.81 m/s^2$. The magnitude of displacement (Y), necessary to achieve a required acceleration at a given frequency is determined by the relationship shown in Equation 10, given that the motion is sinusoidal and periodic. Equation 11 gives an expression for a sinusoidal displacement input.

$$Y = \frac{ag}{(2\pi f)^2} \tag{10}$$

$$y = Y \sin(2\pi f t) \tag{11}$$

The transmissibility, TR,(Transmissibility) of the system, is a measure of the force or motion transmitted through the system. This is shown mathematically in Equation 12. For a linear system, the transmissibility can be derived analytically and is shown in Equation 13, where f_n represents the natural frequency of the system.

$$TR = \frac{|x|}{|y|} \tag{12}$$

$$TR = \frac{1}{1 - (\frac{f}{f_n})^2} \tag{13}$$

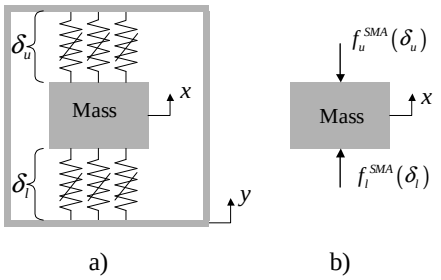

Figure 9. a) Schematic of pseudoelastic SMA spring-mass isolation system b) Free body diagram of pseudoelastic SMA spring-mass isolation system

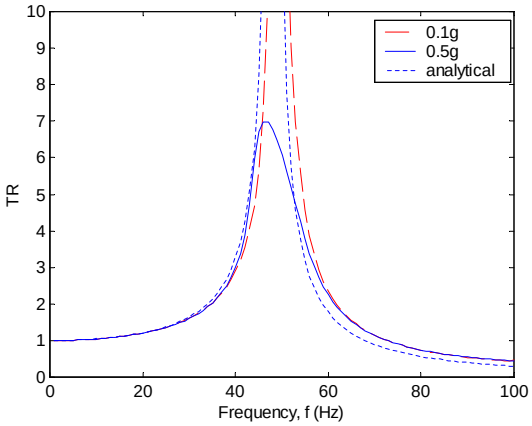

Figure 10: Transmissibility of SMA spring-mass system with different amplitude of base excitation for 1kg mass

With the response of the SMA springs defined, it is now possible to model the system as depicted in Figure 9 and described by Equation 8. Time history response of the system was calculated using a Newmark integration scheme[25] with time step and weighting factors determined to ensure stability of both the integration and the adapted Preisach model describing the SMA spring element behavior.

3.2. Simulation Results

Figure 10 shows the effect of varying the amplitude of base excitation on transmissibility of the SMA spring-mass system. These results are shown for a mass of 1kg, an SMA spring configuration of two upper SMA springs and two lower SMA springs, and a pre-compression of 1mm for all the springs. At lower amplitude of base excitation, the SMA spring-mass system exhibits resonance at a frequency of approximately 48Hz, similar to the transmissibility of a linear system which is shown in Figure 10 by the line labelled "analytical". This can be explained by looking at the force-displacement diagram for one of the SMA springs, as shown in Figure 11. For an excitation amplitude of 0.1g, it is observed that after a few loading cycles the SMA spring repeatedly loads and unloads along a path having a stiffness of approximately 23KN/m, giving a combined total stiffness of approximately 92KN/m. For a mass of 1kg, this equates to a natural frequency of approximately 48Hz. As the excitation amplitude increases, the decrease in stiffness and hysteresis of the SMA's pseudoelasticity begin to contribute to a reduction in the resonant amplitude of the system.

Figure 12 gives the force-displacement history for an excitation amplitude equal to 0.5g at the natural frequency. A wider hysteresis loop is observed due to increased phase transformation, which is a result of higher excitation amplitude, and results in a lower transmissibility (see Figure 10). Figure 13a shows the system response (displacement history) for 0.1g excitation amplitude at resonance and is similar to the response of a linear spring due to the lack of phase transformation, which results in a linear force-displacement relationship. At frequencies greater than resonance frequencies, the system dynamics allow for significant reductions in

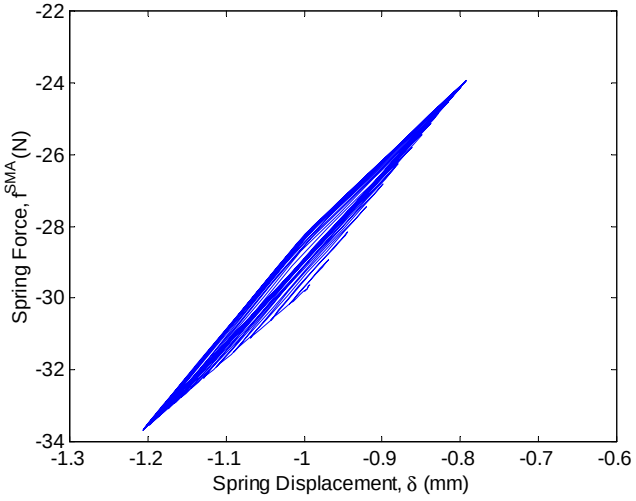

Figure 11. Force-displacement response for an SMA spring for the system with 1kg mass and 0.1g excitation amplitude

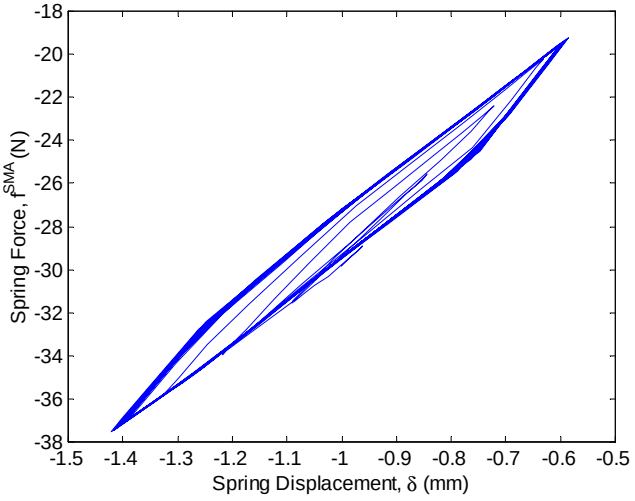

Figure 12. Force-displacement response for an SMA spring for the system with 1kg mass and 0.5g excitation amplitude

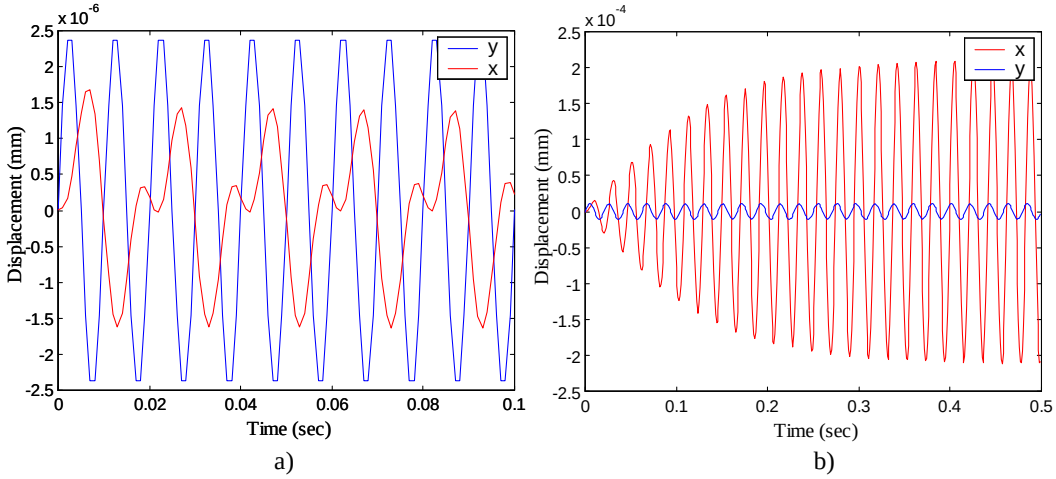

Figure 13. a) System response at resonance for 1kg mass and 0.1g excitation b) System response for 1kg mass, 4 springs, 1.0g excitation amplitude showing reduction in transmissibility utilizing SMAs (100 Hz)

transmissibility, as shown in Figure 13b. From these results, it can be summarized that the greatest benefit of SMA pseudoelasticity can be gained for this system under higher loading levels and near the resonant frequency of the system. It is also important to understand that in order to have vibration isolation with SMA springs, the SMA springs should undergo large amplitude displacement that will result in phase transformation. This will allow the system to operate with a lowered effective spring stiffness, due to the pseudoelastic effect, and will allow the inherent hysteresis present in the SMAs to provide energy dissipation. The SMA force-displacement response should be as close as possible to the major loop behavior as discussed earlier in order to have the most effective vibration isolation.

Effect of increasing mass on transmissibility reduces the resonant frequency of the system and increases the amount of phase transformation as the SMA springs are subjected to higher loads. The effect of changes in the spring configuration results in a predictably lower resonance frequency for the system with fewer springs due to the lower overall stiffness. It should be noted that, for the cases presented, a relatively small amount of pseudoelasticity is observed, especially when compared to the major loop response shown in Figure 8. For

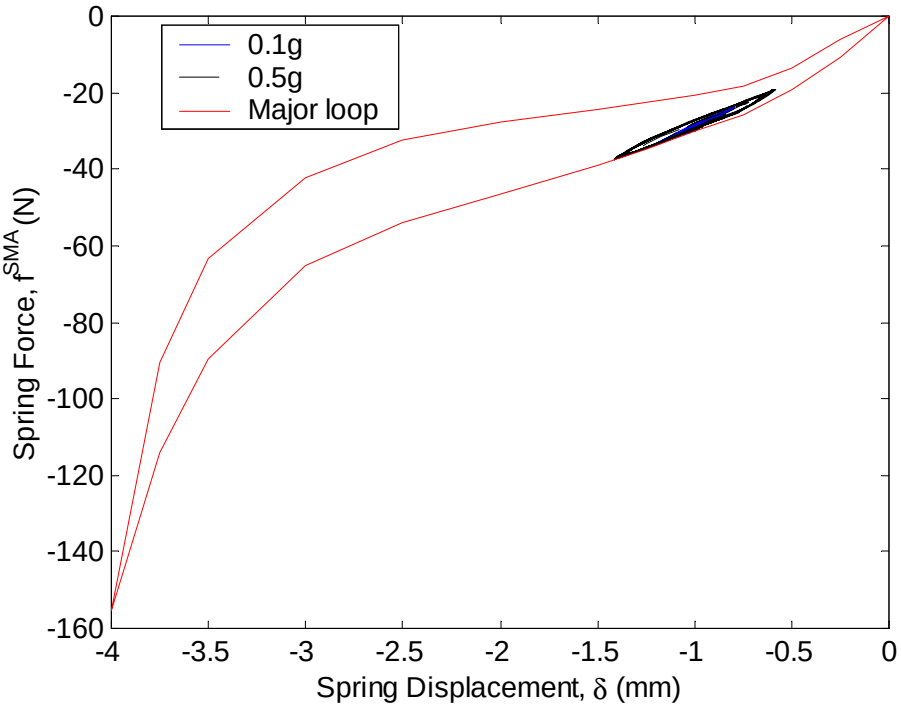

Figure 14: Comparision of major loop hysteresis to minor loop hysteresis induced by system motion for several cases

comparison, the major loop force-displacement relationship and the force-displacement histories shown in Figures 11 and 12 are plotted together in Figure 14. It is evident that greater benefit could be gained from the pseudoelastic effect if larger portions of the force-displacement relationship could be exploited.

4. CONCLUSIONS

In this work, a Preisach model for pseudoelastic SMA force-displacement response has been presented. This model has been utilized to numerically simulate the response of a dynamic system having SMA springs for vibration isolation. In terms of modeling, the classical Preisach operator was adopted for this work to minimize implementation effort. The identification implementation method adopted, helped in mitigating noise amplification in the experimental identification data and simplified the implementation of the Preisach model. The methodology followed, made the Preisach model a useful and accurate tool for simulating the dynamic system motivated from the prototype device referenced earlier. Simulation results of a generic dynamic system show that vibration isolation is greatly dependent on the relative displacement of SMA springs, as this directly affects the extent of phase transformation attained. A detailed parametric study to investigate optimal conditions for passive vibration isolation for the prototype system are under way, to improve the design of the prototype system. Comparison between the model predictions and actual experimental results of the prototype system will be addressed in future work. Based on the theoretical work presented here and specifically on the outcome of numerical studies conducted, it appears that Shape Memory Alloys would be successful candidates for use in a passive vibration isolation device.

ACKNOWLEDGMENTS

The authors would like to acknowledge the financial support the U.S. Air Force - Kirtland AFB, PO No. 00-04-6837 under the administration of Syndetix, Inc., and the Air Force Office of Scientific Research, Grant No. F49620-01-1-0196. The authors would also like to thank Dr. B. Kyle Henderson at AFRL/VSSV for support during this work.

REFERENCES

1. L. L. Beranek and I. L. Vér, eds., *Noise and Vibration Control Engineering*, New York: John Wiley and Sons, 1992.
2. C. M. Harris, ed., *Shock and Vibration Handbook*, New York: McGraw-Hill, 1996.
3. K. Otsuka and K. Shimizu, "Pseudoelasticity and shape memory effects in alloys," *International Metals Review* **31**(3), pp. 93–114, 1986.
4. K. Otsuka and C. M. Wayman, "Introduction," in *Shape Memory Alloys*, K. Otsuka and C. M. Wayman, eds., ch. 2, pp. 27–48, Cambridge, United Kingdom : Cambridge University Press, 1999.
5. C. M. Wayman, "Phase transformations, nondiffusive," in *Physical Metallurgy*, R. W. Cahn and P. Haasen, eds., pp. 1031–1075, New York: North-Holland Physics Publishing, 1983.
6. S. Miyazaki, T. Imai, Y. Igo, and K. Otsuka, "Effect of cyclic deformation on the pseudoelasticity characteristics of Ti-Ni alloys," *Metallurgical Transactions* **42**(7), pp. 115–120, 1997.
7. Z. Bo and D. C. Lagoudas, "Thermomechanical modeling of polycrystalline SMAs under cyclic loading, part IV: Modeling of minor hysteresis loops," *International Journal of Engineering Science* **37**, pp. 1205–1249, 1999.
8. E. Graesser and F. Cozzarelli, "Shape-memory alloys as new materials for aseismic isolation," *Journal of Engineering Materials* **117**, pp. 2590–2608, November 1991.
9. H. Ozdemir, *Nonlinear transient dynamic analysis of yielding structures*. PhD thesis, University of California at Berkeley, 1976.
10. M. Achenbach, T. Atanochovic, and I. Muller, "A model for memory alloys in plane strain," *International Journal of Solids and Structures* **22**(2), pp. 171–193, 1986.
11. P. Thomson, G. J. Balas, and P. H. Leo, "The use of shape memory alloys for passive structural damping," *Smart Materials and Structures* **4**, pp. 36–41, March 1995.
12. Z. C. Feng and D. Z. Li, "Dynamics of a mechanical system with a shape memory alloy bar," *Journal of Intelligent Material Systems and Structures* **7**, pp. 399–410, July 1996.
13. R. Fosdick and Y. Ketema, "Shape memory alloys for passive vibration damping," *Journal of Intelligent Systems and Structures* **9**, pp. 854–870, 1998.
14. R. Aberayatne and J. K. Knowles, "Dynamics of propagating phase boundaries: Thermoelastic solids with heat conduction," *Archive for Rational Mechanics and Analysis* **126**(3), pp. 203–230, 1994.
15. Y. C. Yiu and M. E. Regelbrugge, "Shape-memory alloy isolators for vibration suppression in space applications," in *Proc. 36th AIAA/ASME/ASCE/AHS/ASC Conf. Structures, Structural Dynamics, and Materials*, pp. 3390–3398, April 1995. AIAA-95-1120-CP.
16. J. J. Mayes and D. C. Lagoudas, "An experimental investigation of shape memory alloy springs for passive vibration isolation," in *Proc. Conf. AIAA Space 2001 Conference and Exposition*, (Albuquerque, NM), August 2001. submitted.
17. D. C. Lagoudas, M. M. Khan, and J. J. Mayes, "Modelling of shape memory alloy springs for passive vibration isolation," in *Proc. Conf. ASME International Mechanical Engineering Congress and Exposition*, (New York, NY), November 2001.
18. I. Mayergoyz, *Mathematical Models of Hysteresis*, New York : Springer-Verlag, 1991.
19. G. Webb, *Adaptive Identification and Compensation for a Class of Hysteresis Operators*. PhD thesis, Texas A&M University, College Station, TX, May 1998.
20. G. Webb, A. Kurdila, and D. Lagoudas, "Hysteresis modeling of SMA actuators for control applications," *Journal of Intelligent Material Systems and Structures* **9**(6), pp. 432–447, 1998.
21. M. Krasnoselskii and A. Pokrovskii, *Systems with Hysteresis*, Heidelberg, Germany: Springer-Verlag, 1983.
22. D. Hughes and J. Wen, "Preisach modeling and compensation for smart material hysteresis," *SPIE Active Materials and Smart Structures* **2427**, pp. 50–64, 1994.
23. D. L. W. R. B. Gorbet and M. K.A., "Preisach model identification of a two-wire SMA actuator," in *Proc. IEEE International Conf. on Robotics and Automation*, **3**, pp. 2161–2617, (Leuven, Belgium), May 1998.
24. "MATLAB version 5.3.1.29215a (R11.1) ,1999." The Mathworks Inc. Natick, MA.
25. N. M. Newmark, "A method of computation for structural dynamics," *Journal of Engineering Mechanics Division, ASCE* **85**, pp. 67–94, 1959.